Dispersal and survival of chub mackerel (*Scomber Japonicus*) larvae in the East China Sea

Yuesong Li [a,e], Xinjun Chen [a,e,*], Changsheng Chen [b,a], Jianzhong Ge [c], Rubao Ji [d], Rucheng Tian [b], Pengfei Xue [b], Liuxiong Xu [a,e]

[a] *College of Marine Sciences, Shanghai Ocean University, Shanghai, China*
[b] *School for Marine Science and Technology, University of Massachusetts-Dartmouth, New Bedford, MA 02742, USA*
[c] *State Key Laboratory for Estuarine and Coastal Research, East China Normal University, Shanghai, China*
[d] *Department of Biology, Woods Hole Oceanographic Institution, Woods Hole, MA 02543, USA*
[e] *The Key Laboratory of Sustainable Exploitation of Oceanic Fisheries Resources, Ministry of Education, 999 Hucheng Ring Road, Shanghai 201306, China*

ABSTRACT

An early life stage individual-based model of chub mackerel (*Scomber japonicus*) (IBM-CM) is developed and coupled with the East China Sea (ECS) unstructured grid Finite-Volume Community Ocean Model (FVCOM). Using this coupled physical-biological model, we examined the influences of regional physical processes on the dispersion and survival of chub mackerel larvae in the ECS under climatological spring–summer temperature and circulation conditions with and without the inclusion of short-time fluctuations of a typhoon. The model results show that the seasonal variability of regional circulation, vertical stratification, and mixing play critical roles in larval dispersal and abundance distributions during the early life stages. Sensitivity experiments suggest that under the same physical environment, the larval dispersal distributions and survival rates can be significantly influenced by the location of spawning ground. The impact of a typhoon on the larval transport depends on its path, intensity, speed and timing since most typhoons swept the ECS over a time scale of a few days. The comparison of the cases with and without inclusion of Typhoon Alice indicates that cancelation of tidally-induced anti-cyclonic and typhoon-driven cyclonic currents in the ECS could limit the influence of the typhoon on the low-frequency flow and thus on larval dispersion in this region, but typhoon-enhanced vertical mixing could significantly increase larval mortality and thus decrease the abundance of surviving larvae in the nursery ground in the ECS.

© 2014 Elsevier B.V. All rights reserved.

1. Introduction

It is well recognized that natural environmental variability has a pronounced influence on fish recruitment, particularly on their early larval stages (Bartsch and Coombs, 2001, 2004). In addition to bottom-up (food availability) and top-down (predation pressure) mediation, ocean circulation, water temperature and stratification, and mixing can directly affect larval dispersion, growth, and mortality and thus larval survival rate. Chub mackerel (*Scomber japonicus*), a coastal pelagic species, is widely distributed on the continental shelf in the tropical and subtropical regions of the Pacific, Atlantic and Indian Oceans (Tang, 2006). In the East China

Sea (ECS) and the Japan/East Sea (JES), chub mackerel are classified into two regional stocks: (1) the Tsushima Current (TS) stock and (2) the ECS stock (Yamada et al., 1986). In the purse-seine fishery, the TS stock is more commercially valuable than the ECS stock (Hwang and Lee, 2005). As with many living marine resources, the chub mackerel fishery stocks are subject to fishing pressures, with yield and recruitment considerably influenced by natural environmental factors (Bartsch and Coombs, 2004; Daskalov, 1999).

The current research on chub mackerel is mainly focused on age and growth studies (Gluyas-Millan et al., 1998), resource and environmental dynamics (Hiyama et al., 2002; Watanabe and Yatsu, 2004) and stock assessments (Hill and Crone, 2006), with little consideration of the fluctuation driven by the temporal and spatial variability of the physical environment. In the ECS, the early life of chub mackerel is composed of five life stages: eggs, early larvae, larvae, early juvenile and juvenile (Hunter and Kimbrell, 1980). The early larvae grow slowly in the first 10–15 days until reaching about

* Corresponding author at: College of Marine Sciences, Shanghai Ocean University, Shanghai, China.
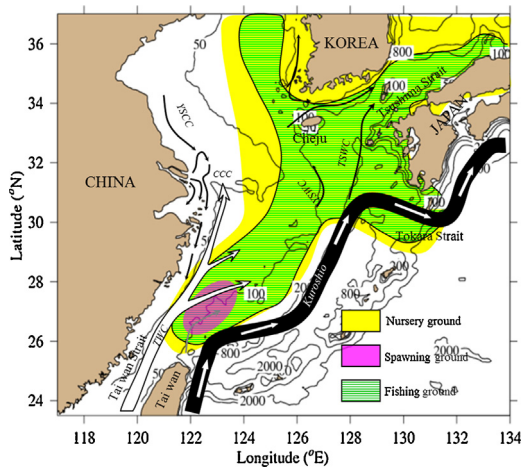*E-mail address:* xjchen@shou.edu.cn (X. Chen).

Fig. 1. Estimated spawning and nursery grounds of the Tsushima Current stock superimposed on the bathymetric map of the East China Sea (ground areas are redrawn based on those displayed in Yukami (2007)). The arrows indicate the regional summertime circulation patterns in the Yellow and East China Seas. YSCC: the Yellow Sea Cold Current; YSWC: the Yellow Sea Warm Current; TSWC: the Tsushima Strait Warm Current; CCC: the Changjiang Coastal Current; and TWC: the Taiwan Warm Current. The circulation patterns were redrawn following Chen et al. (2008).

6–7 mm, followed by rapid growth. When the larvae reach ∼15 mm over a period of 20 days, metamorphosis to the early juvenile stage occurs. The spawning grounds of the Tsushima Current stock are in the northern waters off Taiwan (Fig. 1), with a spawning period from February to June (Yukami et al., 2009). Spawning occurs in the upper 10 m of the water column (Fritzsche, 1978), with substantial influence of the local and regional circulation on dispersion and survival of mackerel larvae.

Circulation, stratification and mixing in the ECS are controlled by complex physical processes associated with the Kuroshio, the Changjiang River discharges, tides and air–sea interactions (Chen et al., 1994) (Fig. 1). The Kuroshio, a warm and saline current, enters the ECS east of Taiwan, flows northeastward along the edge of the continental slope, and then moves eastward into the interior of the Pacific Ocean off the Tokyo coast. The Taiwan Warm Current (TWC) originates from the Taiwan Strait, flows northeastward over the continental shelf, and then separates into two branches: one flowing toward the inner shelf off the Changjiang and the other toward the Tsushima/East Strait. The Changjiang Coastal Current (CCC) forms as a result of the Changjiang River discharge and flows southward along the Chinese coast. The ECS features a strong semidiurnal tide, particularly in the shallow region over the continental shelf (Choi, 1984). The air–sea interactions influence vertical stratification in the ECS, which is vertically well-mixed in the shallow coastal region due to surface cooling and wind mixing during winter, and re-stratified due to surface heating in the summer. Circulation in the ECS varies significantly from season to season as a result of the Changjiang River discharges, winds and cooling/heating. The Kuroshio acts as a retention mechanism to keep the mackerel larvae over the continental shelf of the ECS, while the combined CCC, TWC and monsoon winds tend to advect larvae eastward over the continental shelf to the Tsushima/East Strait. Since these physical processes vary significantly in space and time, they can have a direct impact on the recruitment of chub mackerel in the ECS. What level of influence do the regional circulation and stratification have on the survival rate, dispersion and abundance of mackerel larvae? In addition, the ECS is a subtropical region with frequent disturbance by typhoons, particularly during spring and summer (Chen and Qin, 1985). Typhoons cause strong cyclonic currents and vertical mixing along their pathways when sweeping the ECS. If a typhoon

appears during spawning and early larvae stages, is it a hazard to the mackerel larvae? These questions, to our knowledge, have not been thoroughly examined yet.

Investigation of environmental impacts on mackerel recruitment can be approached by either observational field ecology with statistical correlation techniques (Hiyama et al., 2002) or fully coupled physical-fishery models (Werner et al., 1993; Miller et al., 1998). Built on the Lagrangian theory, the individual-based model (IBM) is a state-of-the-art traditional tool to incorporate the physical processes (such as advection and turbulent mixing) into the behavior of individual larvae in their early life stages (Bartsch and Coombs, 2004; Tian et al., 2009a). The IBM approach is appropriate for application to fisheries ecology when theoretical frameworks have been constructed on growth, mortality and energy flow (Bartsch et al., 2004; Sassa et al., 2008; Wang et al., 2013). To our knowledge, no IBM has been developed to study recruitment of the chub mackerel in the ECS.

The circulation model of the ECS has been continually refined (e.g. Choi, 1984; Yanagi and Takahashi, 1993; Chang and Isobe, 2003; Chen et al., 2008). An unstructured-grid, three-dimensional, primitive-equation, Finite-Volume Community Ocean Model (FVCOM) was applied to the ECS (hereafter referred to as ECS-FVCOM) by Chen et al. (2008). The non-overlapped triangular mesh provides increased resolution of complex irregular coastal geometry and steep bottom topography in the ECS. The volume-conservative, finite-volume algorithm makes this model suitable for biological applications in which mass conservation is prerequisite. Built on the success of ECS-FVCOM development, we have developed an IBM of chub mackerel (hereafter referred to as IBM-CM) and coupled it to ECS-FVCOM. Using this coupled physical-biological model, we examined the influence of the physical environment on the survival and distribution of chub larvae in the ECS.

This paper summarizes the development of the coupled high-resolution ECS-FVCOM and IBM-CM system and presents new findings from process-oriented experiments. It is the first study of this kind in the East China Sea with a focus on examining the impact of the regional-scale physical environment and typhoons on the early life of mackerel larvae. The remaining sections are organized as follows. In Section 2, the coupled model is introduced. In Section 3, the design of process-oriented numerical experiments is described. In Section 4, the model results for 1-D and 3-D experiments are presented, in which the experiments were made for the climatological physical conditions and a selected typhoon event. Discussion and conclusions are followed in Section 5.

2. The coupled ECS-FVCOM and IBM-CM

2.1. ECS-FVCOM

The ECS-FVCOM was developed by Chen et al. (2008), with continual enhancements by the joint research team of the University of Massachusetts-Dartmouth, the East China Normal University and the Shanghai Ocean University (Xue et al., 2009; Ge et al., 2012). The detailed structure of this model was described by Chen et al. (2008) and Xue et al. (2009). The computational domain of ECS-FVCOM covers the entire ECS, Yellow Sea (YS), Bohai Sea (BS), and Japan/East Sea (JES) (Fig. 2), with a horizontal resolution in the range of 1–15 km. The model uses a hybrid coordinate in the vertical, with a total of 40 layers. An s-coordinate with five uniform layers (a thickness of 2 m) near both the surface and bottom is used in the region of >80 m depth, transitioning to a σ-coordinate at a depth of 80 m, which results in a vertical resolution of 2 m or less in the shallower regions. This hybrid coordinate helps the model to resolve the surface mixed and bottom boundary layers.
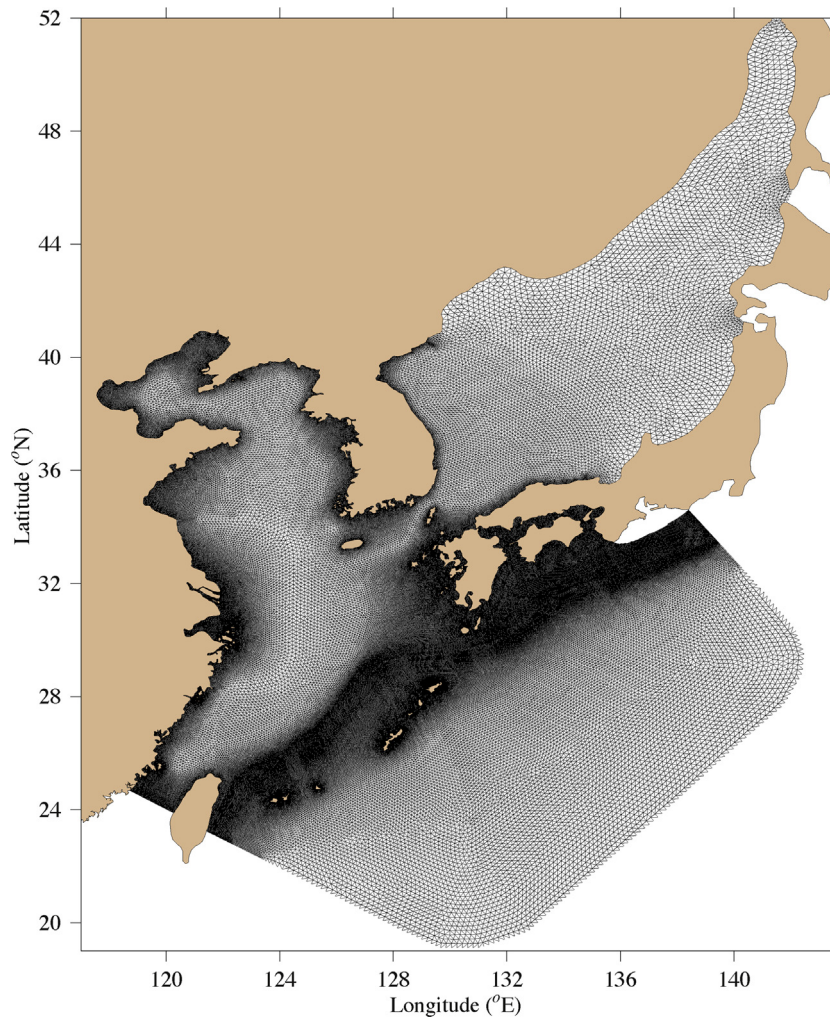
Fig. 2. Unstructured grid of the ECS-FVCOM.

ECS-FVCOM was driven by (1) the tidal forcing constructed using eight tidal constituents (M_2, S_2, N_2, K_2, K_1, P_1, O_1 and Q_1) at the open boundary, (2) climatologic surface forcing (wind stress, net heat flux plus shortwave irradiance, sea level atmospheric pressure gradient, and precipitation minus evaporation) and (3) climatologically averaged monthly freshwater discharges from the Changjiang River. The boundary condition for the Kuroshio is similar to Chen et al. (2008) except that we consider seasonal variation in this study. The vertical viscosity was computed using the Mellor and Yamada level-2.5 turbulence closure model (Mellor and Yamada, 1982), and the horizontal diffusion coefficient was determined using Smagorinsky's turbulent closure scheme (Smagorinsky, 1963). The model was spun up with initial conditions of the January temperature and salinity fields and then integrates conditions from February to July. The model-predicted 3-D fields of water temperature, currents and vertical viscosity were used to drive the IBM-CM.

2.2. IBM-CM

We describe the IBM-CM here by following a general ODD ("Overview", "Design concept" and "Detail") protocol (Grimm et al., 2006).

2.2.1. Purpose

The IBM-CM is developed to simulate the early life ecology of chub mackerel larvae. This model covers five life stages from spawning and egg incubation to juveniles.

2.2.2. State variables and scales

Individuals were characterized by the state variables: age (in days), location (in three dimensions: longitude, latitude and depth), life stage (eggs, early larvae, larvae, early juvenile and juvenile) and status (alive or dead). The physical environment was characterized by three-dimensional oceanic currents (unit: m/s), temperature (unit; °C), vertical eddy viscosity (unit: m^2/s) and horizontal eddy diffusion (unit: m^2/s). The state variables track properties of individual mackerel larvae (Appendix) over the five life stages, with lengths from ∼1 mm to ∼130 mm and a time scale up to 4 months.

2.2.3. Process overview and scheduling

Individuals were tracked by the Lagrangian model constructed from the 3-D flow field of the ECS-FVCOM. Due to a large number of eggs and larvae, "super-individuals" were utilized. In the Lagrangian tracking program, a super-individual is defined as an ensemble particle with a total number of 10^9 individuals (as used in Tian et al., 2009a). Each individual included the state variables described above. The growth of individual larvae is a function of age, standard length, food availability, and water temperature. Mortality rates were assumed to be inversely correlated with larval length. The empirical equations of growth and mortality, which include metamorphosis, food availability and water temperatures, at each life stage are listed in Appendix.
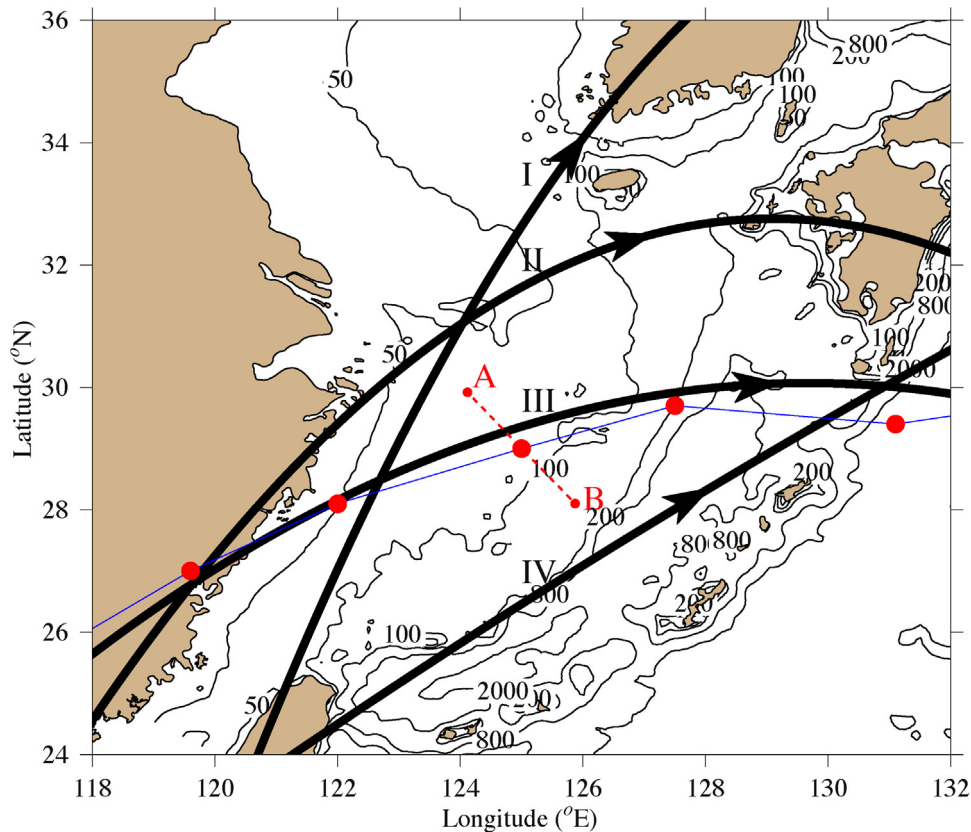
Fig. 3. Statistics of typhoon paths over the ECS summarized based on typhoon records from April to May 1949–2009. Blue line: Typhoon Alice's path in May 1961. The red dashed line labeled A and B is the transect where a comparison was made for the surface mixed layer in the cases with and without inclusion of Typhoon Alice.

2.2.4. Design concepts

The empirical functions used to describe the five early life stages from egg incubation to juveniles are based on laboratory and field measurements. The duration for each stage was set up based on previous studies. In this study, our focus is on the impact of the seasonal climatological physical condition and severity of typhoon events on the dispersal and survival of mackerel larvae. The movements of individuals were fully controlled by a 3-D Lagrangian flow and turbulence (individual random walk) (see Eqs. (2) and (3)), with no diel and seasonal vertical migration process considered.

2.2.5. Initialization

The IBM-CM was initialized at spawning of chub mackerel. The spawning stock was specified following Yamada et al. (1998) and Yukami (2007), which was assumed to be 10^6, in which 65% were female. Three ages (1, 2, and >3) of females were considered, at spawning rates of 60%, 85% and 100%, respectively. Spawning of these females covered the period from February to June, with a peak in April (Yamada et al., 1998; Liu et al., 2005). During that period, individual females spawn every 5.7 days over a 36-day period, for a total of 6.3 times. This setup followed the estimation by Yamada et al. (1998), with average fecundity for an individual female of 0.55 million eggs during a single spawning season. In the IBM-CM, we assumed that the spawning of individual females satisfied a normal distribution function (Tian et al., 2009b) given as

$$e_i(t) = N_m S_e \int_{t_0}^{t} \frac{1}{\sqrt{2\pi}\sigma} e^{-(1/2)(t-t_M/\sigma)^2} \tag{1}$$

where $e_i(t)$ is the number of eggs spawned by the ith individual female at time t, N_m is the total number of female mackerel, S_e is the total number of eggs spawned by each individual adult mackerel in a spawning season, t_0 is the start time of spawning, t_M is the
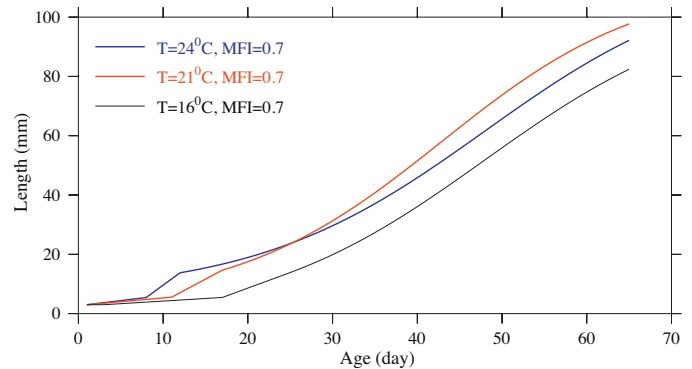

Fig. 4. Larval length (mm) vs. larval age (day) at water temperatures of 16 °C, 21 °C and 24 °C for a given MFI of 0.7.

maximum spawning time that was specified to be 20 days (480 h) and σ is the standard deviation specified as 5.7 days (136 h). When the total egg number reached 10^9 individuals, they formed a super particle.

It should be pointed out that in this study our focus was on examining the impacts of physical environments on early life stages of mackerel larvae after spawning, so the number of eggs and the method of spawning by individual females were not critical. For this reason, we simplified our approach by following Yamada et al.'s (1998) work, with a major focus on peak spawning periods of individual females. Also, it should be noted that the experiments were made using a super-particle approach. Although individual females could spawn over four months, egg numbers were significantly lower in nonpeak periods, and no significant individual super particles could form.
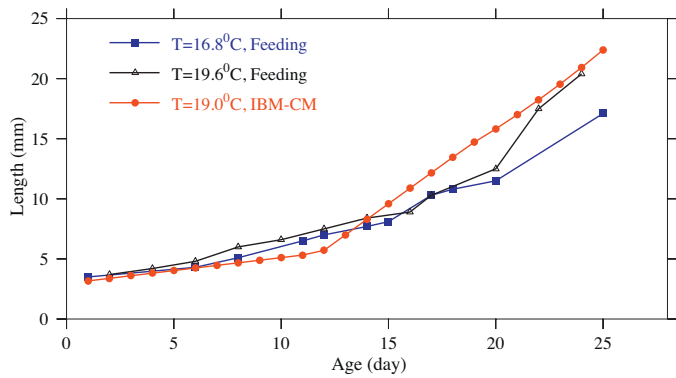
Fig. 5. Comparison of larval length (mm) vs. larval age (day) under feeding and IBM-CM simulation conditions.
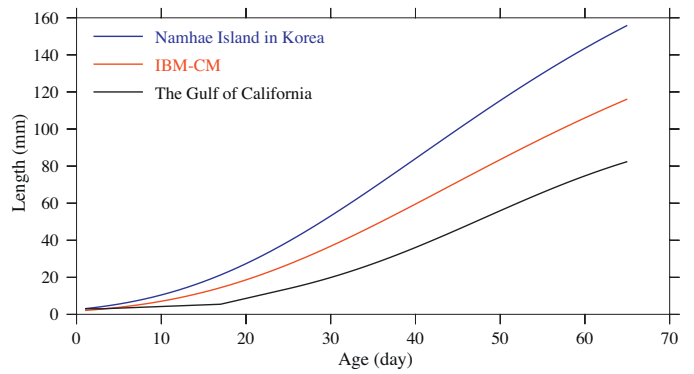
Fig. 6. Comparison of the IBM-CM-predicted larval length with simulation results for Namhae Island, South Korea (Hwang, 2005) and the Gulf of California, Mexico (Gluyas-Millan et al., 1998).
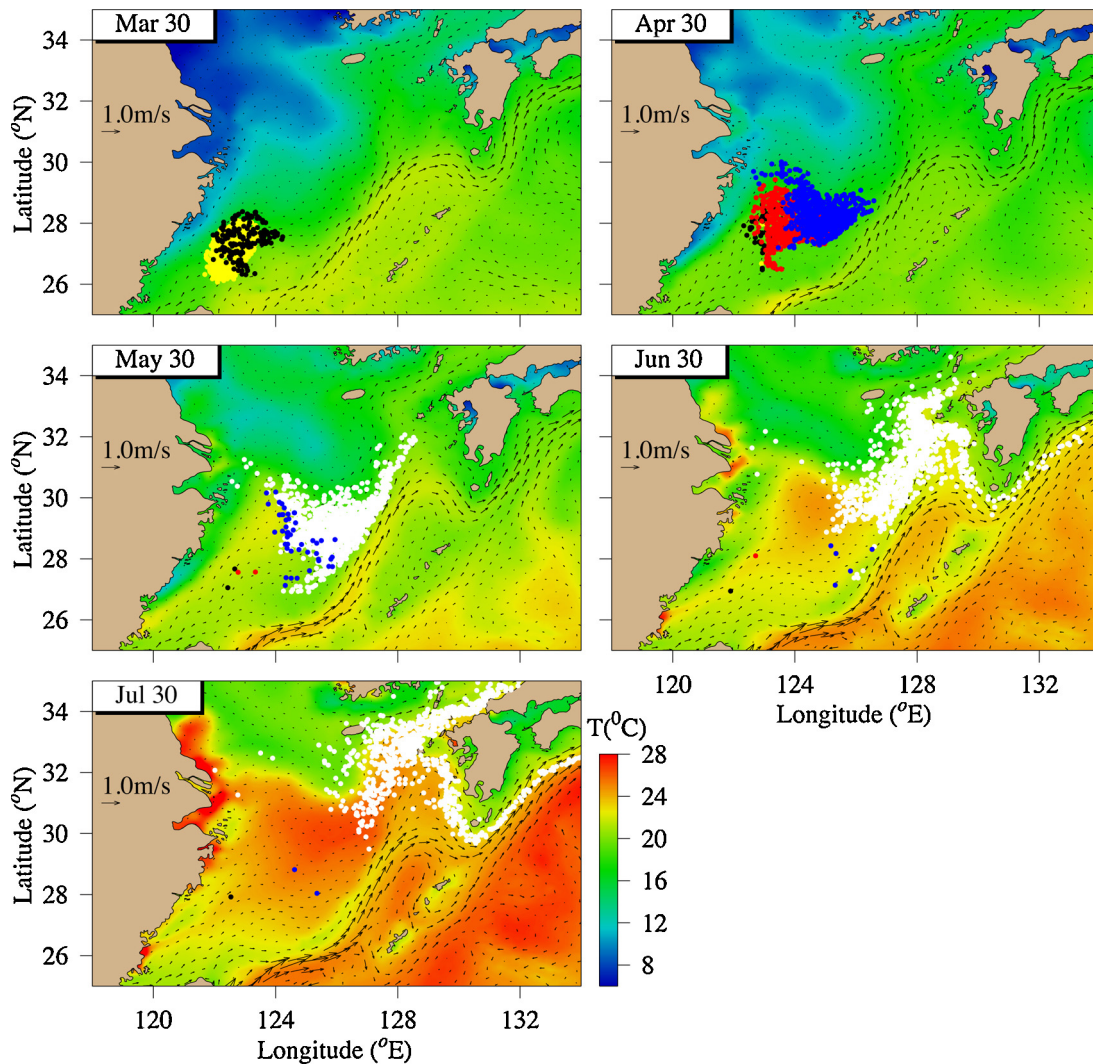

Fig. 7. Dispersal of mackerel larvae superimposed on the surface regional circulation and water temperature on the 30th of March, April, May, June and July under climatological physical conditions. Vectors: the subtidal near-surface currents, and colors: the sea surface temperature. Yellow dot: egg stage; black dot: early larvae stage; red dot: larvae stage; blue dot: early juvenile stage; and white dot: juvenile stage. (For interpretation of the references to color in this figure legend, the reader is referred to the web version of the article.)

2.2.6. Input

The 3-D flow fields, water temperature, vertical eddy viscosity, horizontal mixing coefficients, and upwelling index were the physical variables input from the ECS-FVCOM. At each life stage, the biological parameters controlling growth and mortality were specified based on our understanding of the ecology of mackerel larvae in the ECS.

2.2.7. Submodels

The super-individuals were tracked following the 3-D flow field plus turbulence-induced random walk in the form of

$$P_n(\vec{x}, t) = \int_{t-\Delta t}^{t} \vec{v}dt + R(K_m) + P(\vec{x}_{t-\Delta t}, t - \Delta t) \qquad (2)$$

where $P_n(\vec{x}, t)$ and $P_n(\vec{x}_{t-\Delta t}, t - \Delta t)$ are the locations of the nth super-individual at t and $t - \Delta t$; $\vec{v}$ is the 3-D velocity vector; $R(K_m)$ is the vertical random walk distance during the Δt time interval; and K_m is the vertical eddy viscosity output directly from the ECS-FVCOM. The advective distance was calculated by a modified fourth-order Runge–Kutta time-stepping scheme with second-order accuracy (Chen et al., 2003). A vertical random walk was simulated following Visser's (1997) differential equation with a time step of δt. Defining $\hat{n}$ as the random walk time step at $t - \Delta t$, the vertical location of the nth super-individual caused by the random walk after δt was computed by

$$z_{\hat{n}+1} = z_{\hat{n}} + K'_m \delta t + r[2\sigma_2^{-1} K_m(z_{\hat{n}} + 0.5 K'_m \delta t)]^{1/2} \qquad (3)$$

where $K'_m = \delta K_m / \delta z$, r is a random process with a zero mean, and σ_z is the standard deviation. K_m varies in space and with time. In the ECS-FVCOM simulation, K_m was a sum of background mixing coefficient and turbulence-closure model-calculated vertical eddy viscosity. It was of an order of magnitude of 10^{-5} m^2/s in the thermocline of the Kuroshio, 10^{-3}–10^{-4} m^2/s in the mixed layer, and 10^{-2} m^2/s in a vertically well-mixed shallow region. During the typhoon event, K_m was up to 10^{-2} m^2/s in the mixed layer. Assuming that r is a uniform distribution between +1 and −1, $\sigma_z = 1/3$. To avoid unrealistic aggregation of super-individuals, the random walk generator required that δt be much smaller than Δt (the Lagrangian integral time scale) (Chen et al., 2003). In this study, $\Delta t = 120$ s, and $\delta t = 6$ s, so that $R(K_m) = z_{\hat{n}+20} - z_{\hat{n}}$, where $z_{\hat{n}}$ is the vertical location of the nth super-individual at $t - \Delta t$.

All equations for growth, mortality and food limitation at each life stage are provided in Appendix, with descriptions from the literature used to derive these equations.

3. Design of numerical experiments

We first conducted an experiment of IBM-CM in the absence of the 3-D flow and temperature fields to examine quantitatively the effects of water temperature, food and feeding on growth of larvae during their early life stages. Then we used ECS-FVCOM-computed physical flow and water property fields to drive the IBM-CM to study how the spatial and temporal variability of physical fields affect the dispersion, settlement and survival of larvae during the early life stages.

Two physical conditions were considered: (1) the climatological condition in which the physical fields were produced by running ECS-FVCOM under climatological meteorological forcing conditions from March to July and (2) the climatological condition with the inclusion of a typhoon event. The purpose of the second experiment was to examine the impacts of tropical storms, which occur over the ECS frequently during spring and summer, on dispersal and settlement of mackerel larvae. We collected all records of typhoons that swept over the ECS during April–May from 1949 to 2009. All typhoons originated from the South China Sea and swept across the
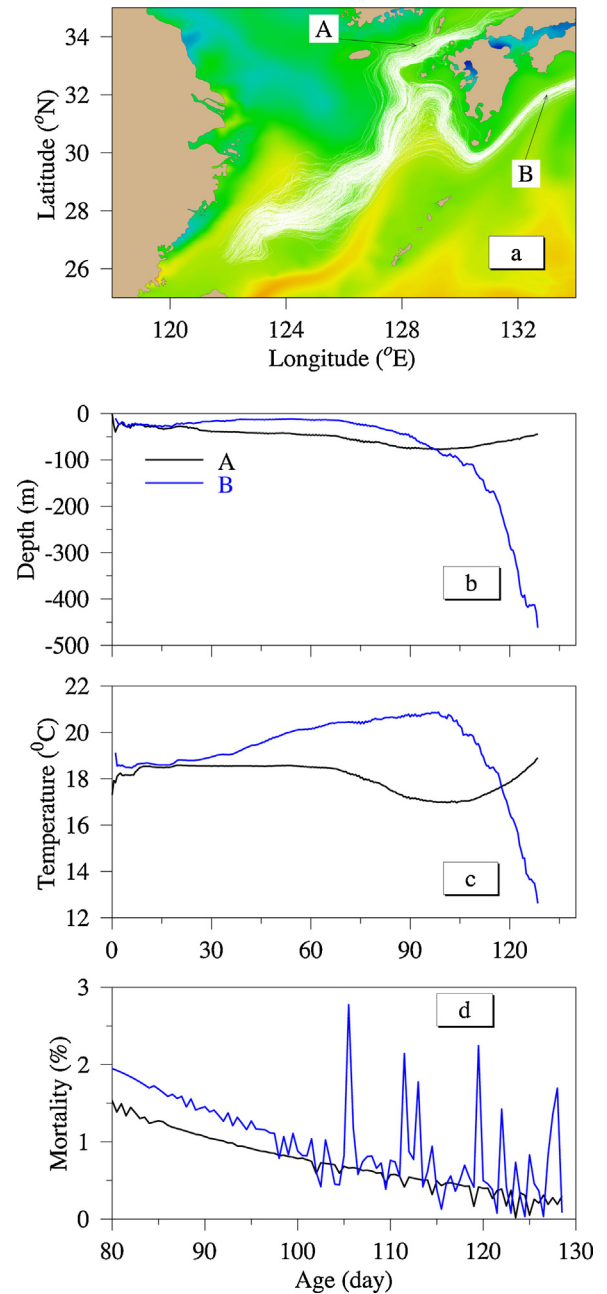

Fig. 8. Illustration of group A (entering the Tsushima/East Strait) and group B (drifting with the main stream of the Kuroshio to the eastern coast of Japan). (a) Paths of group A and group B; (b) the mean water depths along the paths; (c) the mean water temperature along the paths; (d) mean larval mortality by age along the paths.

ECS following four major paths (Fig. 3). The spawning zone of chub mackerel was located over the shelf, south of 28°N. It appears that typhoons that followed path III had greater influence than the other three because they occurred within the mackerel larval dispersal region shown in Fig. 1. To run the model with a realistic typhoon, we selected Typhoon Alice as an example of the path III typhoons. Typhoon Alice swept over the ECS shelf on 18–21 May 1961, with a maximum wind speed of ~28 m/s and a low pressure of 995 hPa. For the Typhoon Alice case, the model run started on 1st March under climatological forcing conditions, with wind and pressure fields for Typhoon Alice added at 18:00 PM on May 18. The typhoon made landfall around 18:00 PM on May 21. After that, the wind field was returned to the climatological condition.
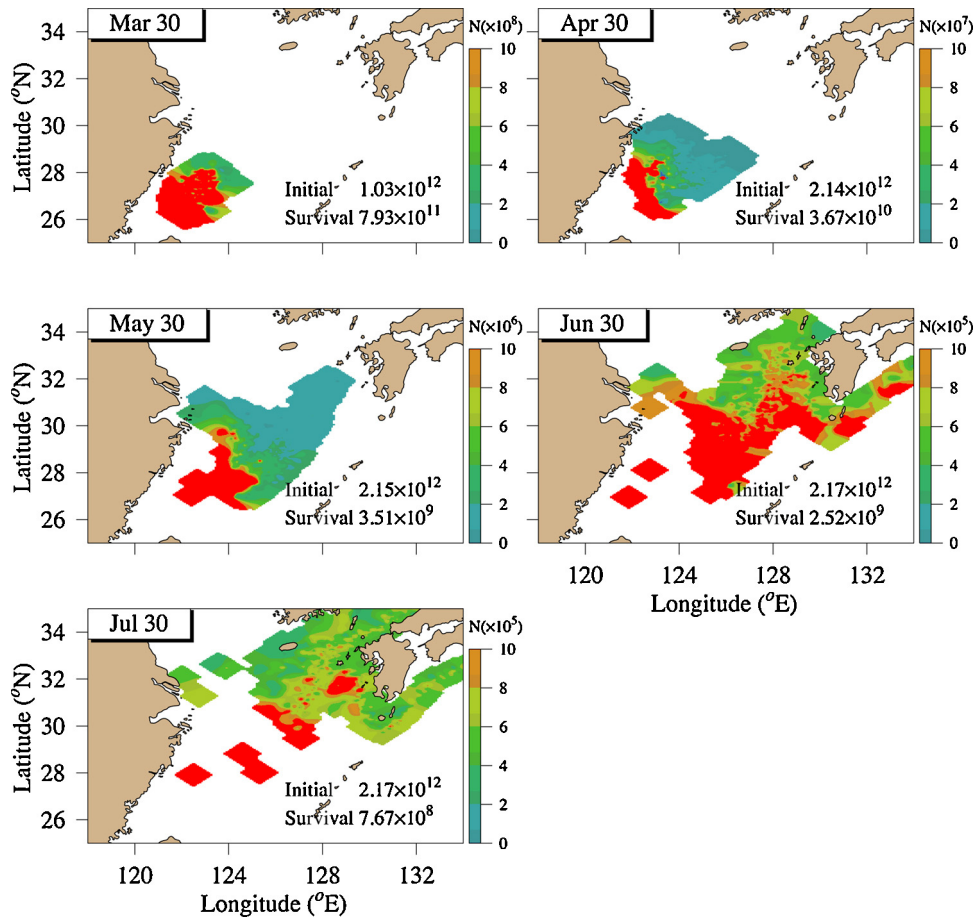
Fig. 9. Spatial distributions of larval abundances on the 30th of March, April, May, June and July under climatological physical conditions.

Dispersion of mackerel larvae was sensitive to circulation in the ECS. Since the flow system was so complex in that region, the dispersal and survival rates of mackerel larvae could significantly differ among the cases in which eggs were spawned in different spawning regions. To gain a more general knowledge of the impact of the physical environment on early life stages of mackerel larvae in the ECS, we performed sensitivity experiments by shifting the location of the spawning ground to the east, west, north and south by a distance of 60 km. These experiments were made with the climatological flow condition.

4. Results and discussions

4.1. The idealized IBM-CM experiments

Temperature and food played significant roles in early larval developmental stages. Over the continental shelf of the ECS, the water temperature during March–July varied from 16° to 28 °C. In the absence of the 3-D flow and temperature fields, we ran the IBM-CM with water temperatures of 16°, 20° and 24 °C under the same model food index (MFI) of 0.7 to examine the impact of water temperature change on incubation and metamorphosis time. With a constant food index between simulations (MFI = 0.7), the model indicated that both incubation and metamorphosis time decreased with water temperature, with values of 3.52 and 25.7 days, respectively at 16 °C, 1.81 and 17.73 days at 20 °C, and 1.31 and 12.95 days at 24 °C. Correspondingly, the standard larval lengths after the two-month simulation were 70, 90 and 80 mm, respectively (Fig. 4). In egg, early larvae and larvae stages (about 15 days), the growth was positively correlated with temperature, while in early

juvenile and juvenile stages, the growth was positively correlated with an optimal temperature ($\sim$20 °C). This result was consistent with the faster growth at an optimal temperature (20 °C) observed in the laboratory experiment.

Food availability was calculated using the coastal upwelling index (CUI). This index was determined by the upward water velocity of ECS-FVCOM: a standard indirect indicator of environmental enrichment (Fur and Simon, 2009). Larval feeding encounter rate increased with upward water velocity (Rothschild and Osborn, 1988). Following the approach of Hunter and Kimbrell (1980) for *S. japonicus* laboratory-rearing studies, we compared the growth rate of the IBM-CM ($T = 19$ °C, MFI = 0.8) with laboratory growth rates at 19.6 °C and 16.8 °C after hatching (Fig. 5). In the laboratory rearing, the larvae grew faster as the temperature increased. In the IBM-CM, the larval growth rate was considered an environmental factor, which did not follow linearly with the temperature. Compared with the laboratory results, the larval growth rate was lower in the first 13 days and then higher after that. The model simulation growth rate coincided with the range of those found at Namhae Island in South Korea (Hwang and Lee, 2005) and the Gulf of California in Mexico (Gluyas-Millan et al., 1998) (Fig. 6).

4.2. The 3-D ECS-FVCOM- and IBM-CM experiments

4.2.1. The climatological forcing conditions

Driven by the February–July climatological forcing, we tracked super-individuals from spawning to the juvenile stage. Fig. 7 shows the larval dispersal on the continental shelf of the ECS on March 30, April 30, May 30, June 30 and July 30. (Note that February is not shown in the figure because no significant super-particles
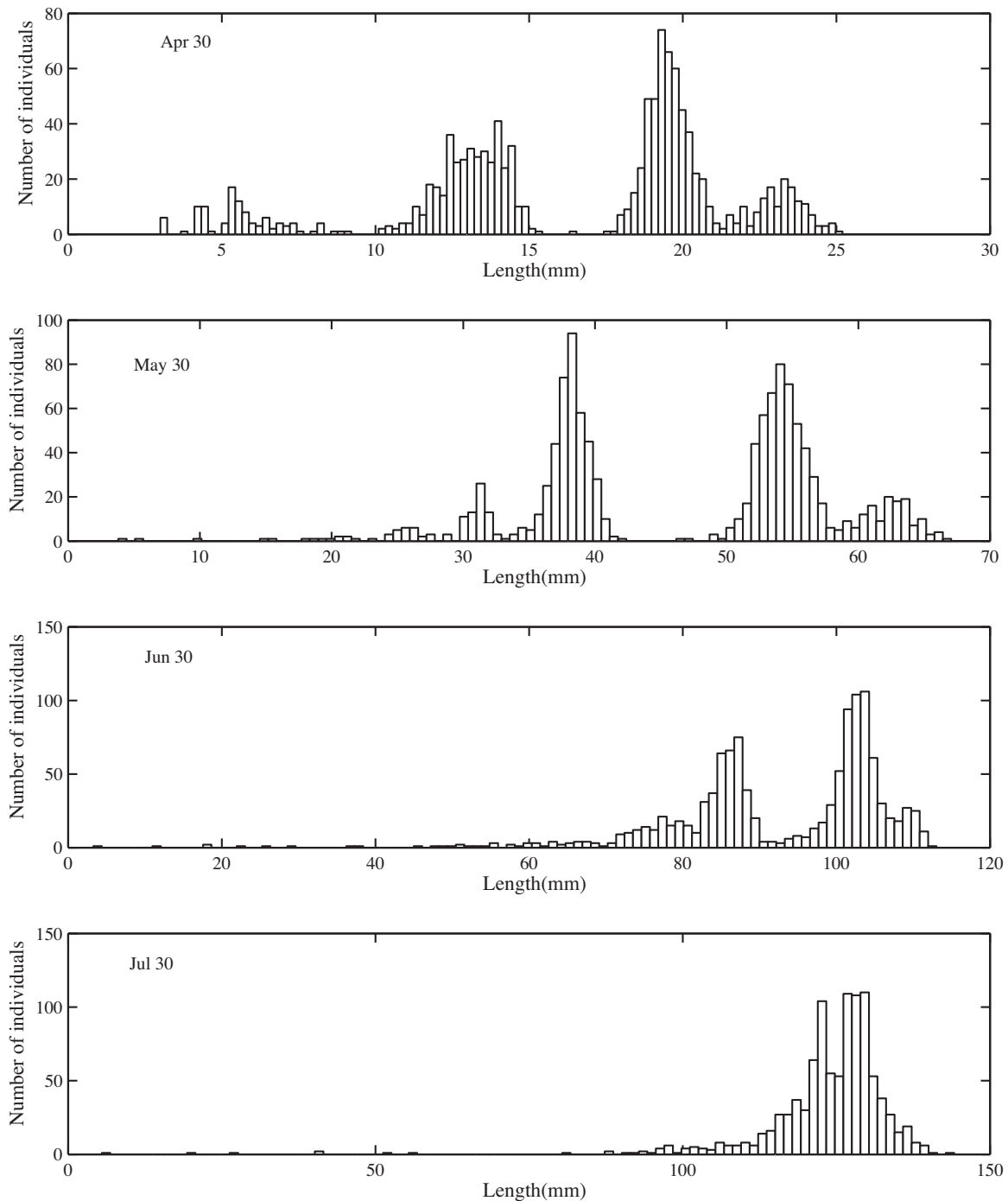
Fig. 10. Frequency histogram of lengths on 30th of April, May, June and July under climatological physical conditions.

formed in that month.) The results indicate that the transport path of larvae was mainly controlled by horizontal advection and vertical diffusion. After spawning, the larvae were generally advected southeastward (between the 50-m and 100-m isobaths) and then northeastward (between the 100-m and 200-m isobaths) over the continental shelf, with a few transported northward to enter the Zhoushan Island complex off Hangzhou Bay. The Kuroshio sped up the northeastward transport in May. The super-individuals were divided into two groups at the Kuroshio bifurcation region southwest of Kyushu in mid and late June: one flowed northeastward to enter the Japan/East Sea through the Tsushima/East Strait, and the other moved southeastward to follow the main stream of the Kuroshio and then flowed along the eastern Japanese coast.

Defining larvae drifting to Tsushima/East Strait as group A and larvae drifting into the main stream of Kuroshio east of the Japanese coast as group B (Fig. 8a), we compared mean water depths, temperatures and mortalities with respect to larval ages (Fig. 8b and c). The bifurcation of these two groups occurred after 90 days. After that, group A remained in the upper 100 m where the water temperature was 17 °C or higher, while group B was transported deeper into an unfavorable nursery region in which the water temperature dropped from ∼20 °C to ∼12 °C (Fig. 8b and c). Correspondingly, the mortality was about 0.5% or lower for group A, but fluctuated up to ∼2.8% for group B (Fig. 8d).

Fig. 9 shows the distribution of larval abundance at the end of each month from March to July. It is clear that the Kuroshio
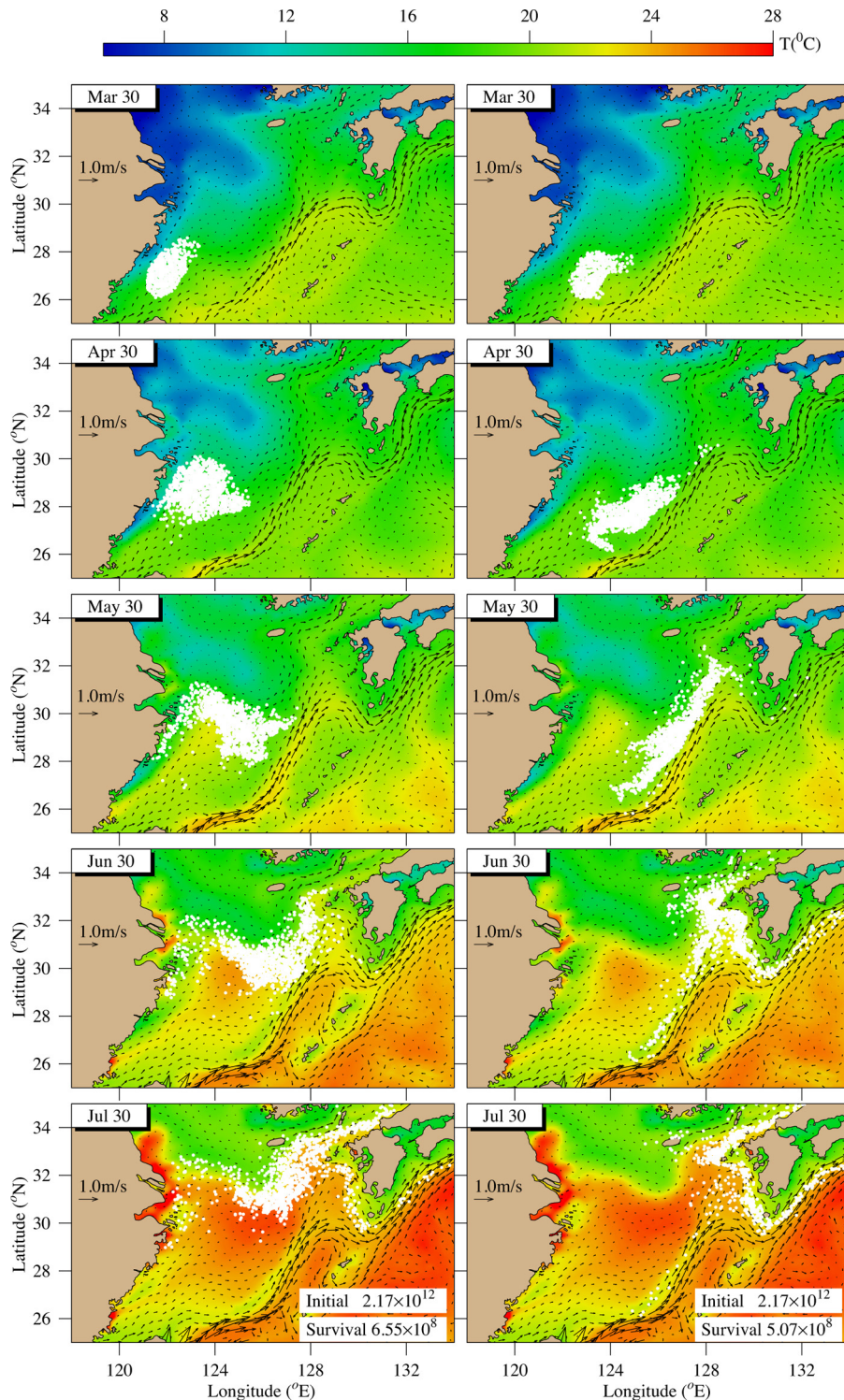
Fig. 11. Dispersal of mackerel larvae superimposed on the surface regional circulation and water temperature on the 30th of March, April, May, June and July for case-WSG and case-ESG. Vectors: subtidal near-surface currents; colors: sea surface temperature; white dot: mackerel larvae.

acted like a barrier that restricted larvae from being advected to the interior of the western Pacific Ocean, while the flow over the continental shelf moved larvae northeastward from the Chinese shelf toward the coast of Japan. In such a physical environment, the larval abundance was higher over the continental shelf. In June, the highest abundance occurred in the southwestern region of Kyushu, with bifurcated distributions following group A and group B.

The number of individuals with respect to larval length varied with time due to different spawning times and advection in a time-varying physical environment. The length histogram (Fig. 10) indicates that there were several abundance peaks as a result of the batch-spawning reproductive strategy of chub mackerel. On May 30, for example, two distinct juvenile groups with lengths of 30–40 mm and 50–60 mm were observed. On July 30, all surviving individuals had a length of 100–150 mm.
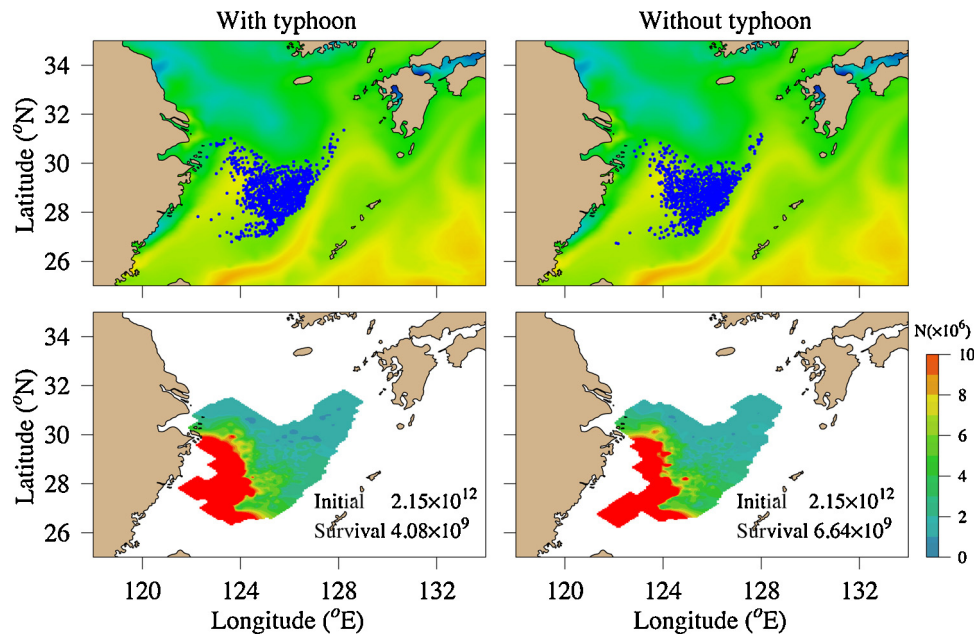
Fig. 12. Dispersal of larvae on May 21 with and without the inclusion of Typhoon Alice (above); spatial distributions of larval abundances (below).

The model-predicted larval dispersal was consistent with the temporal and spatial distributions of the Tsushima Current stock shown in Fig. 1 (summarized by Yukami et al., 2009). The regional circulation was a key mechanism for linking the northeast of Taiwan spawning and Tsushima fishing grounds. Larval dispersal from the northeast of Taiwan had a direct impact on the Tsushima fishing ground, but little influence on the fishing grounds in the Changjiang estuary and Zhou-Shan islands.

4.2.2. Sensitivities to spawning grounds

Larval dispersal and survival could significantly differ as the location of spawning grounds changed (Fig. 11). By shifting the spawning grounds 60 km to the east and west, alternately, we found that the pathways of patchily-distributed larvae dramatically differed from those shown in Fig. 7. In the case with a spawning ground shifting 60 km to the west, larvae were advected northward by the Taiwan Warm Current during February–April, and then turned anticyclonically onto the plateau area east of the submerged valley off the Changjiang estuary in May. These larvae were not able to reach the main stream of the Kuroshio in June. Instead, they were advected northeastward toward the Tsushima/East Strait when close to the Kuroshio at around 126°E. Similar to the scenario shown in Fig. 8, the super-individuals were also separated into two groups at the Kuroshio bifurcation region southwest of Kyushu, but this occurred a few weeks later. As a result, more larvae were transported to the nursery area around Cheji Island in July (Table 1).

Table 1
Proportion of larvae (*Scomber japonicus*) arriving in the four nursery grounds for case-SSG, case-WSG and case-ESG.

Nursery grounds	Experiments		
	Case-WSG	Case-SSG	Case-ESG
Tsushima/East Strait	0.10	0.19	0.18
The Pacific	0.05	0.20	0.36
Cheju Island	0.79	0.46	0.27
Kyushu Island	0.06	0.15	0.19

In the case of the spawning grounds shifted 60 km to the east, the larval dispersion was strongly affected by the Kuroshio. In this case, no larvae could be advected to the near-shore region of the ECS. Most larvae followed the Kuroshio Current to drift northeastward at a faster speed. Once these larvae entered the Kuroshio bifurcation region, they were then separated into two groups like those shown in Fig. 8, but the individuals were much larger for group B than for group A (Table 1).

No significant differences were found by shifting the spawning grounds 60 km to the north or to the south, so no descriptions of that variation are presented in this paper. Defining the results presented in Fig. 7 as a "standard spawning grounds" case (hereafter referred to as "case-SSG") and those described in Fig. 11 as "western and eastern spawning grounds" cases (hereafter referred to as "case-WSG" and "case-ESG", respectively), we counted the proportion of larvae arriving in four nursery grounds (Table 1). Clearly, only the 60-km difference in the location of spawning grounds could result in significantly different proportions of larval abundance in these four regions. Shifting the spawning ground coastward produced a high arrival rate in the nursery ground around Cheju Island, while shifting the spawning ground to the Kuroshio could result in greater larval transport to the Pacific (eastern Japanese coast) and thus lead to high mortality. We also counted the abundance of surviving individuals by the end of July for these three cases. They were 7.67×10^9 for case-SSG, 6.65×10^9 for case-WSG and 5.07×10^9 for case-ESG. Dividing by the total number of individuals at beginning of the spawning season, we estimated the larval survival rates at 0.0353%, 0.0306% and 0.0234%, respectively. The low survival rate found for case-ESG was due to the transport of a larger portion of larvae to the east Japanese coast.

4.2.3. Typhoon impacts

The impacts of a typhoon on larval dispersal in the ECS depended on the storm's intensity, path, and duration. Incorporating Typhoon Alice into the FVCOM simulation, we compared the model-predicted larval dispersal after Alice passed the ECS with that predicted for the case-SSG under the climatological forcing condition. No significant difference was found in larval dispersal for these two cases (Fig. 12), but a difference was evident in larval
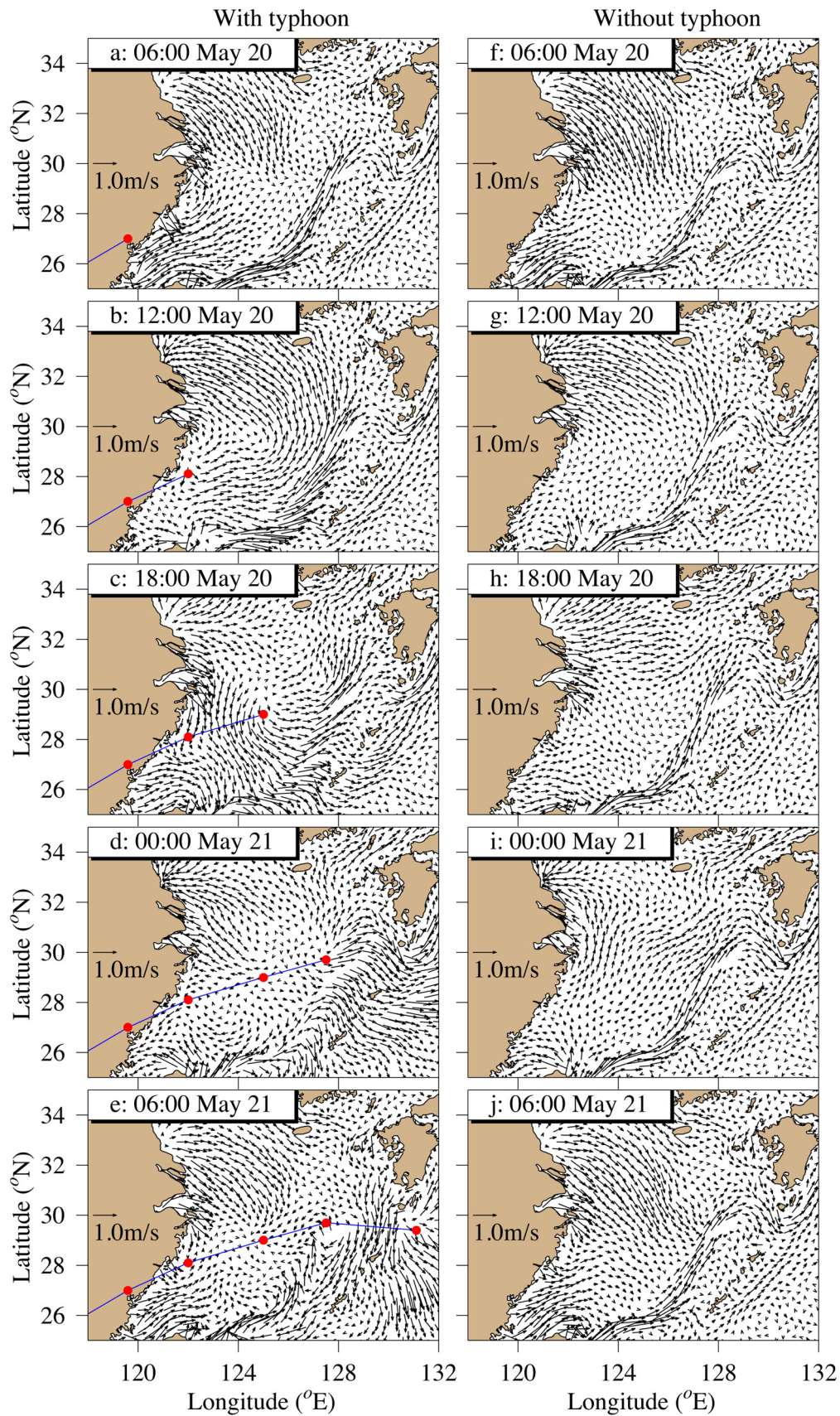
With typhoon　　　　　　　　　Without typhoon

Fig. 13. The ECS-FVCOM-predicted flow fields with (a–e) and without (f–j) the inclusion of Typhoon Alice on May 20–21.
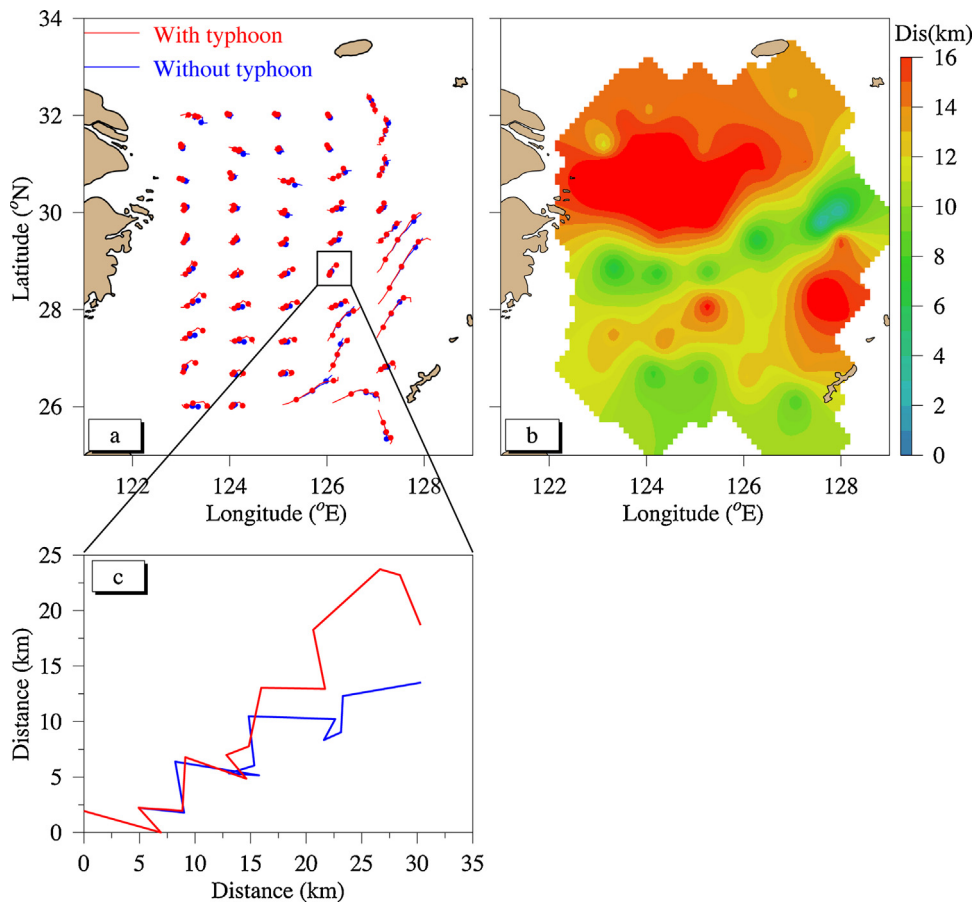
Fig. 14. Trajectories of super-individuals with and without the inclusion of Typhoon Alice (a); spatial distance difference distributions in the simulation final stage (b); an enlarged view of a super-individual's trajectories (c).

abundances. The typhoon significantly increased the larval mortality rate, with larval abundance by the end of July at 6.65×10^9 in case-SSG, but decreased to 4.06×10^9 in the case with the inclusion of Typhoon Alice.

The ECS continental shelf features semi-diurnal M_2 tidal currents, that rotate anticyclonically over a period of 12.42 h. Tidal currents over the continental shelf are on the order of 20–50 cm/s (Guo and Yanagi, 1998). Typhoon Alice swept the ECS in a short period of ~2 days and the water currents produced by this typhoon were of the same order of magnitude as the M_2 tidal currents. In this particular case, the cancelation of typhoon-induced cyclonic and tidally induced anticyclonic currents resulted in a small effect on the residual flow: a low-frequency current that transported larvae. This cancelation process can be seen in Fig. 13, where the near-surface currents were modified by Typhoon Alice. Such a change, however, did not produce a significant modification of larval movement over two days. To further investigate this result, we performed an additional experiment by tracking 50 particles released at the sea surface under conditions with and without the inclusion of Typhoon Alice. Results showed no obvious change of trajectories in the larval transport paths compared to the typhoon (red line) and climatological wind (blue line) paths (Fig. 14a). On the larval transport path, the change of trajectories was smaller (Fig. 14b), with a typhoon-induced dispersal scale of only about 5 km (Fig. 14c).

A significant reduction in larval abundance after the typhoon was believed to be a result of strong vertical mixing. Fig. 15 shows a comparison of depths of the surface mixed layer on a transect A–B

(see Fig. 3) for the cases with and without the inclusion of Typhoon Alice. For the case without the typhoon, a thin surface mixed layer formed in mid-May as the surface heat flux increased. The thickness of this layer varied from a few meters at site A to 20 m at site B. When Typhoon Alice was considered, the strong wind associated with the typhoon significantly enhanced vertical mixing. As a result, the surface mixed layer deepened from 10 m at site A to 40 m or deeper at site B. Over the continental shelf between site A and site B, strong wind fluctuation increased the mixed layer depth to >50 m. The enhanced vertical mixing produced a larger vertical eddy viscosity, which directly influenced the random walk generation. Although the vertical distribution of larvae maintained similar patterns for the cases with and without the typhoon, the typhoon-induced enhancement of vertical mixing caused large fluctuations beneath the mixed layer, and hence led to a higher mortality of larvae.

The impact of a typhoon on the dispersal of larvae depended on its duration in the ECS. Alice was a fast-moving typhoon with a short duration of ~2 days. Over such a short period, its influence was minor. If we decreased the speed of this typhoon to increase its duration to 5 days, we observed that the typhoon-induced cyclonic circulation tended to move larvae northwestward onto the shelf region off the Changjiang River, with increased mortality. As a result, the abundance of surviving larval individuals dropped to 3.67×10^9, about 0.39×10^9 (11%) less than that with a short duration of 2 days. There is no question but that such a change would directly affect the recruitment of mackerel larvae and thus its yield in the Japan/East China Sea.
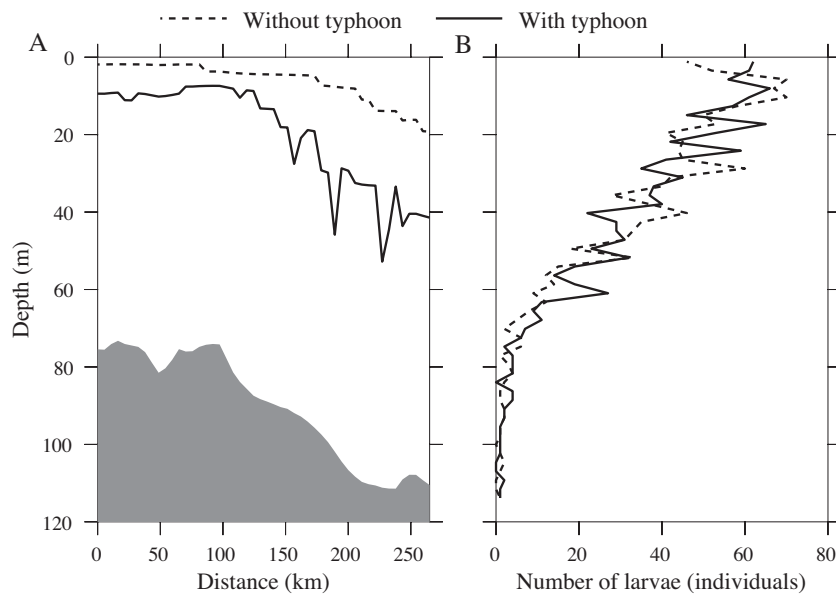
Fig. 15. Comparisons of the thickness of the surface mixed layer along the transect A and B (left panel) and the vertical distribution of the larvae (right panel) around that transect between the cases with and without Typhoon Alice (left panel).

5. Summary

We have developed an IBM-CM and coupled it with the ECS-FVCOM for the study of the early life stages of mackerel larvae in the ECS. Under climatological physical conditions, the transport of larvae was mainly controlled by horizontal advection, lateral dispersion and vertical diffusion. After spawning in the northern shelf region of Taiwan over a period starting in February, the larvae were generally advected southeastward and then northeastward over the continental shelf. The larvae were divided into two groups at the Kuroshio bifurcation region southwest of Kyushu: one that flowed northeastward to enter the Japan/East Sea through the Tsushima/East Strait, and another that moved southeastward to follow the main stream of the Kuroshio and then flowed along the eastern Japanese coast. Larvae that entered unfavorable nursery areas along the eastern coast of Japan could undergo reduced growth and potentially result in death.

Dispersal and settlement of mackerel larvae could significantly differ as the location of the spawning grounds changes. A difference of only 60 km in the location of the spawning ground could result in significantly different proportions of larval abundance in the four nursery grounds. Shifting the spawning ground westward produced a high arrival rate in the nursery grounds around Cheju Island, while shifting the spawning ground eastward could result in enhanced larval transport to the eastern Japanese coast and thus lead to high mortality.

The impact of a typhoon on larval dispersal in the ECS depended on its intensity, path, and duration. In the case of Typhoon Alice, which swept the nursery area over the continental shelf of the ECS over a period of ∼2 days, the cancelation of typhoon-induced cyclonic and tidal-induced anticyclonic currents resulted in a small influence on the residual flow and thus larval transport, but the typhoon-induced strong vertical mixing increased larval mortality and thus reduced the abundance of surviving larvae.

The results of our process-oriented experiment suggest that altering spawning grounds and periods can have varied impacts on larval dispersal and growth in the ECS. Success in reproducing the spawning and nursery grounds of the Tsushima Current stock demonstrated that a coupled ECS-FVCOM and IBM-CM model can be used to address questions of survival and recruitment of

mackerel larvae in the ECS. The Tsushima Current stock is originally spawned on the northern shelf of Taiwan and advected over the continental shelf along the Kuroshio path, indicating that the upwelling index assumption for the food field works well as a first-order approximation. This assumption, however, may not be applied to the spawning grounds off the Changjiang River or other places where horizontal advection and vertical mixing play an essential role in the distribution of prey items. Incorporation of a food web model into the IBM-CM is needed to increase biological relevance. The field measurements suggest that juveniles have locomotory ability, negating the assumption of passive dispersal at this stage. This factor should be considered in the future study of the recruitment of mackerel larvae in the ECS.

It should be pointed out that our experiments did not consider the diel and seasonal vertical migration of chub mackerel larvae. It is evident that chub mackerel adults migrate in the vertical over a day–night cycle. However, it is unclear that the mackerel larvae had the same diel vertical migration behavior as mackerel adults. Since no observational data on the diel vertical migration of larvae were available when the experiments were made, was not taken into account. This aspect should be considered in the future study of chub mackerel recruitment.

Appendix. A five-stage early life history model of chub mackerel larvae (IBM-CM)

The IBM-CM was developed based on the five early life stages. In this individual-based model, larval growth and mortality were functions of age and standard length. The mathematics used to simulate each stage is given below.

Stage I: The incubation time of eggs ranged from 33 h at 23 °C to 117 h at 14 °C in laboratory conditions (Hunter and Kimbrell, 1980). The incubation time (H) was given as

$$H = 3800 \exp\{-6.68[1 - \exp(-0.0527T)]\} \tag{A.1}$$

where T was the water temperature (°C). Eggs hatch in 2–4 days after spawning at water temperatures of 16–19 °C (Fritzsche, 1978; Hunter and Kimbrell, 1980). Egg mortality was assumed to be 10% per day (Bartsch and Coombs, 2004). In this stage, larvae can reach a 1–3 mm in length.

Stage II: This was a stage in which larvae grew linearly in length up to 6 mm over 2/3 metamorphosis times (m_days). "m_days" was defined as

$$m\_days = 51.168 - 1.593T \tag{A.2}$$

In this stage, the larval mortality in each super-individual was estimated by

$$M = \frac{5.0G^{0.7}}{L^{1.3}} \tag{A.3}$$

where M was the daily mortality rate, G was the absolute growth rate defined as

$$G = rL\left[1 - \left(\frac{L}{L_\infty}\right)\right] \tag{A.4}$$

and L was the larval length in mm at time t; L_∞ was a constant representing the maximum length at the end of the juvenile stage (=110 mm); and r was a function of water temperature (T) and food concentration. r was defined as

$$r = [r_{opt} - d(T_{opt} - T)^2]F_i \tag{A.5}$$

where r_{opt} was the maximum specific growth rate (=0.1185), d was a constant (=0.00082), T_{opt} was the optimal temperature for growth (= 20 °C), and F_i was a model food index (MFI). The absolute growth rates and mortality rates were positively correlated. Mortality rates were inversely correlated with larval length, decreasing as larval length increases.

Stage III: This was an early larval stage during which larvae grew rapidly up to ~15 mm in length during 1/3 m_days (about 16–24 days within the local temperature range). Rays in the second dorsal, anal and pelvic fins were fully formed. The growth was described by a function given as

$$L(t + 1) = L(t) + \frac{9.0}{\sqrt[3]{m\_days/24}} \tag{A.6}$$

where $L(t+1)$ and $L(t)$ were larval lengths at time steps of $t+1$ and t. In this stage, the larval mortality was specified by (A.3).

Stage IV: After metamorphosis, the larval growth was calculated by a logistic curve specified as

$$L = L_\infty[L + \exp(-rt + c)]^{-1} \tag{A.7}$$

where c was a constant integral (=3.6). This growth function was derived by Bartsch and Coombs (2001, 2004). The time scale for this stage was ~30 days, and larvae grew into the early juvenile stage with lengths up to 30 mm. In this stage, the water temperature and food were generally considered as the most important parameters of population dynamics and individual growth (Thompson, 1982).

Stage V: This was a stage during which early juveniles grew into juveniles by following the same growth and mortality rates described in stage IV. The time scale was about 30 days. At the end of this stage, larvae can reach a length of ~80 mm.

In this study, MFI was estimated using the coastal upwelling index (CUI). In coastal physical oceanography, the CUI was defined as the wind-induced offshore transport normalized to the local isobath (unit: m^3/s) (Bakun, 1973). In our study, we defined CUI as a non-dimensional parameter in the form of

$$CUI = \frac{w_i - w_{min}}{w_{max} - w_{min}} \tag{A.8}$$

where w_{max} and w_{min} are the maximum and minimum vertical velocities respectively in the computational domain at a larval tracking time step; w_i is the vertical velocity of the ith individual at the same time step when w_{max} and w_{min} were calculated. CUI was in a range from 0 to 1 and determined using the ECS-FVCOM-predicted vertical velocity. This index was a standard indirect indicator of environmental enrichment via an upwelling: a high level of environmental enrichment was proportional to a high CUI value (Fur and Simon, 2009). We assumed that larval feeding encounter rate increased with upwelling (Rothschild and Osborn, 1988), and MFI was determined directly by CUI in a range from 0 to 1.

References

Bakun, A., 1973. Coastal Upwelling Indices, West Coast of North America, 1946–1971. NOAA Tech. Rep., NMFS SSRF-671., pp. 103.

Bartsch, J., Coombs, S.H., 2001. An individual-based growth and transport model of the early life-history stages of mackerel (*Scomber scombrus*) in the eastern North Atlantic. Ecol. Mod. 138, 127–141.

Bartsch, J., Coombs, S.H., 2004. An individual-based model of the early life history of mackerel (*scomber scombrus*) in the eastern North Atlantic, simulating transport, growth and mortality. Fish. Oceanogr. 13, 365–379.

Bartsch, J., Reid, D., Coombs, S.H., 2004. Simulation of mackerel (*scomber scombrus*) recruitment with an individual-based model and comparison with field data. Fish. Oceanogr. 13, 380–391.

Chang, P.H., Isobe, A., 2003. A numerical study on the Changjiang diluted water in the Yellow and East China Sea. J. Geophys. Res. 108, 3299, http://dx.doi.org/10.1029/2002JC001749.

Chen, C.S., Qin, Z., 1985. Dynamic analysis of typhoon surges along the east coast of Zhejiang and Jiangsu Provinces. Acta Oceanol. Sin. 4 (4), 516–526.

Chen, C.S., Beardsley, R.C., Limeburner, R., Kim, K., 1994. Comparison of winter and summer hydrographic observations in the Yellow and East China Seas and adjacent Kuroshio during 1986. Cont. Shelf. Res. 14, 909–929.

Chen, C.S., Liu, L., Beardsley, R.C., 2003. An unstructured grid, finite-volume, three-dimensional, primitive equation ocean model: application to coastal ocean and estuaries. J. Atmos. Ocean. Technol. 20, 159–186.

Chen, C.S., Xue, P., Ding, P.X., Beardsley, R.C., et al., 2008. Physical mechanisms for the offshore detachment of the Changjiang Diluted Water in the East China Sea. J. Geophys. Res. 113, C02002, http://dx.doi.org/10.1029/2006JC003994.

Choi, B.H., 1984. A three-dimensional model of the East China Sea. In: Ichiye, T. (Ed.), Ocean Hydrodynamics of Japan and East China Sea. Elsevier, Amsterdam, pp. 209–224.

Daskalov, G., 1999. Relating fish recruitment to stock biomass and physical environment in the Black Sea using generalized additive models. Fish. Res. 41, 1–23.

Fritzsche, R.A., 1978. *Scomber japonicus* Houttuyn, chub mackerel. In: Development of Fishes of the Mid-Atlantic Bight. An Atlas of Egg, Larval and Juvenile Stages, vol. V, Chaetodontidae Through Ophidiidae. U.S. Fish and Wildlife Service, Washington, DC, pp. 106–114.

Fur, J., Simon, P., 2009. A new hypothesis concerning the nature of small pelagic fish clusters. An individual-based modelling study of *Sardinella aurita* dynamics off West Africa. Ecol. Mod. 220, 1291–1304.

Ge, J., Chen, C., Qi, J., Ding, P., Beardsley, R.C., 2012. A dike-groyne algorithm in a terrain-following coordinate ocean model (FVCOM): development, validation and application. Ocean. Model. 47, 26–40.

Gluyas-Millan, M.G., Castonguay, M., Quinonez-Velazquez, C., 1998. Growth of juvenile Pacific mackerel, *Scomber japonicus* in the Gulf of California. Sci. Mar. 62, 225–231.

Grimm, V., Berger, U., Bastiansen, F., et al., 2006. A standard protocol for describing individual-based and agent-based models. Ecol. Mod. 198, 115–126.

Guo, X.Y., Yanagi, T., 1998. Three-dimensional structure of tidal current in the East China Sea and the Yellow Sea. J. Oceanogr. 54, 651–668.

Hill, K.T., Crone, P.R., 2006. Stock Assessment of Pacific Mackerel with Recommendations for the 2005–2006 Management Season (Executive Summary). Pacific Fishery Management Council, June 2006 Briefing Book, Exhibit G.3, Attachment., pp. 177.

Hiyama, Y., Yoda, M., Ohshimo, S., 2002. Stock size fluctuations in chub mackerel (*Scomber japonicus*) in the East China Sea and the Japan East Sea. Fish. Oceanogr. 11, 347–353.

Hunter, J.R., Kimbrell, C.A., 1980. Early life history of pacific mackerel, *Scomber japonicus*. Fish. Bull. 78, 89–100.

Hwang, S., Lee, T., 2005. Spawning dates and early growth of chub mackerel *Scomber japonicus* as indicated by otolith microstructure of juveniles in the inshore nursery ground. Fish. Sci. 71, 1185–1187.

Liu, Y., Yan, L.P., Hu, F., Chen, J.H., 2005. Age and growth of *Pneumatophorus japonicas* in the north of the East China Sea and the south of the Yellow Sea. Mar. Fish. 27 (2), 133–138 (in Chinese with English abstract).

Mellor, G.L., Yamada, T., 1982. Development of a turbulence closure model for geophysical fluid problem. Rev. Geophys. 20, 851–875.

Miller, C.B., Lynch, D.R., Carlotti, F., et al., 1998. Coupling an individual based population dynamic model of *Calanus finmarchicus* to a circulation model for the Georges Bank region. Fish. Oceanogr. 7, 219–234.

Rothschild, B., Osborn, T., 1988. Small-scale turbulence and plankton contact rates. J. Plankton. Res. 10, 465–474.

Sassa, C., Tsukamoto, Y., Nishiuchi, K., Konishi, Y., 2008. Spawning ground and larval transport processes of jack mackerel *Trachurus japonicus* in the shelf-break region of the southern East China Sea. Cont. Shelf. Res. 28, 2574–2583.

Smagorinsky, J., 1963. General circulation experiments with the primitive equations. I. The basic experiment. Mon. Weather Rev. 91, 99–164.

Tang, Q.S., 2006. Marin Biology Resources and Habitat Environments in the EEZ of China. Science Press, Beijing, pp. 599–608 (in Chinese).

Thompson, B.M., 1982. Growth and development of *pseudocalanus elongatus* and *calanus* sp. in the laboratory. J. Mar. Biol. Asses. U.K. 62, 359–372.

Tian, R.C., Chen, C.S., Stokesbury, K.D.E., et al., 2009a. Dispersal and settlement of sea scallop larvae spawned in the fishery closed areas on Georges Bank. ICES J. Mar. Sci. 66, 2155–2164.

Tian, R.C., Chen, C.S., Stokesbury, K.D.E., et al., 2009b. Modeling exploration of the connectivity between sea scallop populations in the Middle Atlantic Bight and over Georges Bank. Mar. Ecol. Prog. Ser. 380, 147–160.

Visser, A.W., 1997. Using random walk models to simulate the vertical distribution of particles in a turbulent water column. Mar. Ecol. Prog. Ser. 158, 275–281.

Wang, Y., Wei, H., Kishi, M.J., 2013. Coupling of an individual-based model of anchovy with lower trophic level and hydrodynamic models. J. Ocean Univ. China 12, 45–52.

Watanabe, C., Yatsu, A., 2004. Effects of density-dependence and sea surface temperature on interannual variation in length-at-age of chub mackerel (*Scomber japonicus*) in the Kuroshio-Oyashio area during 1970–1997. Fish. Bull. 102, 196–206.

Werner, F., Page, F., Lynch, D., Loder, J.W., Lough, R.G., Perry, R.I., et al., 1993. Influences of mean advection and simple behavior on the distribution of cod and haddock early life stages on Georges Bank. Fish. Oceanogr. 2, 43–46.

Xue, P., Chen, C.S., Ding, P.X., Beardsley, R.C., Lin, H., Ge, J., et al., 2009. Saltwater intrusion into the Changjiang River: a model-guided mechanism study. J. Geophys. Res. 114, C02006, http://dx.doi.org/10.1029/2008JC004831.

Yamada, U., Tagawa, M., Kishida, S., Honjo, K., 1986. Fishes of the East China Sea and the Yellow Sea. Seikai Reg. Fish. Res. Lab, Nagasaki.

Yamada, T., Aori, I., Mitani, I., 1998. Spawning time, spawning frequency and fecundity of Japanese chub mackerel *Scomber Japonicus* in the waters around the Izu Islands. Jpn. Fish. Res. 38, 83–89.

Yanagi, T., Takahashi, S., 1993. Seasonal variation of circulation in the East China Sea and the Yellow Sea. J. Oceanogr. 49, 503–520.

Yukami, R., 2007. Report of chub mackerel assessment of Tsushima Current stock in 2007. Seikai National Fisheries Research Institute Bull., pp. 32 (in Japanese).

Yukami, R., Ohshimo, S., Yoda, M., Hiyama, Y., 2009. Estimation of the spawning grounds of chub mackerel *Scomber japonicus* and spotted mackerel *Scomber australasicus* in the East China Sea based on catch statistics and biometric data. Fish Sci. 75, 167–174.